



Analyst

A highly sensitive endotoxin sensor based on redox cycling in a nanocavity

Journal:	<i>Analyst</i>
Manuscript ID	AN-ART-03-2019-000478.R1
Article Type:	Paper
Date Submitted by the Author:	22-Apr-2019
Complete List of Authors:	Ito, Kentaro; Tohoku University, Graduate School of Environmental Studies Inoue, Kumi; Tohoku University, Graduate School of Environmental Studies Ino, Kosuke; Tohoku University, Graduate School of Engineering Matsue, Tomokazu; Tohoku University - Katahira Campus Shiku, Hitoshi ; Tohoku University, Graduate School of Engineering

SCHOLARONE™
Manuscripts

Title**A highly sensitive endotoxin sensor based on redox cycling in a nanocavity**

Kentaro Ito¹, Kumi Y. Inoue^{1*}, Kosuke Ino², Tomokazu Matsue¹, Hitoshi Shiku^{2**}

¹Graduate School of Environmental Studies, Tohoku University, Sendai, Miyagi 980-8576, Japan

²Department of Applied Chemistry, Graduate School of Engineering, Tohoku University, Sendai 980-8579, Japan

Corresponding authors:

*kumi.inoue.b3@tohoku.ac.jp

**hitoshi.shiku.c3@tohoku.ac.jp

Abstract

We report a highly sensitive and rapid electrochemical method for the detection of endotoxin, based on *Limulus* amoebocyte lysate (LAL) assay using redox cycling at a pair of electrodes in a nanocavity for electrochemical signal amplification. Boc-Leu-Gly-Arg-*p*-aminophenol (LGR-pAP), we previously developed as a substrate for the amperometric LAL assay, and newly prepared Z-Leu-Gly-Arg-aminomethylferrocene (LGR-AMF) were examined as a substrate for LAL based endotoxin assay using a nanocavity device. During the last step of endotoxin-induced LAL cascade reaction, pAP or AMF is generated from the substrate, which can be detected electrochemically with efficient signal amplification by redox cycling between the two electrodes in the nanocavity. A device with a 190-nm-high nanocavity was fabricated by photolithography. With the fabricated device, we demonstrated that pAP in model assay solutions prepared by mixing LGR-pAP and pAP can be quantitatively detected by differences in oxidation potential between LGR-pAP and pAP. As for LGR-AMF and AMF, the difference in the formal potential of 0.1 V was considered to be not sufficient to distinguish AMF from LGR-AMF. However, we show for the first time that even in this case, analytes such as AMF can be detected by differences in diffusion coefficients between the analyte and coexisting molecules (such as LGR-AMF) using a device with high redox cycling efficiency. Next, the endotoxin assay was performed using the fabricated nanocavity device. Using this method, endotoxin was detected at concentrations as low as 0.2 and 0.5 EU/L after 1 h and 30 min of LAL reaction time, respectively, using the LGR-pAP substrate. However, the endotoxin assay using LGR-AMF was not successful because the clotting enzyme did not react with LGR-AMF. This problem might be solved by further design of the substrate. Our nanocavity device represents an effective platform for the simple and rapid detection of endotoxin with high sensitivity.

INTRODUCTION

Highly sensitive analytical methods for the detection of biological molecules with a portable device and easy-to-handle detection scheme are increasingly important for various fields including clinical use. Electrochemical methods are prospective candidates applicable to such analytical devices because of their high sensitivity, simplicity, and miniaturized features. Among the various electrochemical methods, redox-cycling-based amperometric techniques in a nanoscale space realize high sensitivity that enables single molecule detection¹. In normal amperometric techniques, a single redox molecule reacts only once at the working electrode. In redox-cycling based methods, a redox molecule oxidized at one electrode diffuses to the other electrode where it is reduced back to its original state. This redox cycling amplifies the electrochemical signal by repeating the reactions at the two electrodes. Since the amplification efficiency increases with decreasing distance between the two electrodes, methods using the nanogaps have achieved sufficient sensitivity to successfully detect a single molecule.¹⁻⁶ Previously, we reported highly sensitive cell evaluation methods using redox-cycling-based electrochemical chip devices with nanocavities.⁷

Endotoxin, a liposaccharide, is an analyte that requires highly sensitive detection for medical safety.⁸ Contamination of injective medicines including dialysate with endotoxin, which is ubiquitous in the environment as a component of the outer membrane of gram-negative bacteria, is a serious problem because only a very small amount of endotoxin initiates the innate immune response inducing septic shock in mammalian cells.⁹ In addition, endotoxin has high chemical and thermal stabilities and should be strictly controlled with monitoring to avoid contamination of medical supplies. For example, from the guidelines presented by Japanese Society for Dialysis Therapy in 2016, the standard established for endotoxin contamination in ultrapure dialysis fluid is <1 EU/L,¹⁰ which coincides with the lowest detection limit of the conventional endotoxin assay. The *Limulus* amoebocyte lysate (LAL) assay is the most commonly used endotoxin detection method, listed in the Pharmacopoeia of the US, EU and Japan. The LAL assay is based on an endotoxin-mediated coagulation pathway associated with a cascade reaction of three protease zymogens. When endotoxin binds to Factor C zymogen, Factor C is activated and subsequently activates Factor B, which cleaves the proclotting enzyme to produce its active form. The resulting clotting enzyme cleaves the chromogenic substrate, promoting yellow color development that can be measured at 405 nm with a spectrophotometer.¹¹ Scudder *et al.* detected 0.025 EU/L within 5 min of LAL reaction time using a more sensitive assay involving photonic-crystal total-internal-reflection.¹² Another highly sensitive endotoxin assay was reported by Takahashi *et al.* using a photonic crystal nanolaser, which detected 1.0 EU/L within 33 min of LAL reaction time.¹³ However, these methods require high-cost equipment and skilled technicians to perform the test. Electrochemical detection is a promising method of providing low-cost, compact, easy-to-use, and highly sensitive assays.¹⁴⁻¹⁹ In

our previous study, 0.5 EU/L of endotoxin was detected with 60 min of LAL reaction time by measuring the response of *p*-aminophenol (pAP) liberated from a pAP-conjugated peptide (Boc-Leu-Gly-Arg-pAP; LGR-pAP) with substitutional stripping voltammetry.¹⁷ This method achieved sufficient sensitivity to be applied for monitoring endotoxin contamination in ultrapure dialysis fluid under the strictest standards, but still required 60 min for detection, which must be shortened for practical use.

In this study, we developed a novel electrochemical method for highly sensitive and rapid endotoxin detection based on the LAL reaction using a nanocavity device for signal amplification by redox cycling. We fabricated a redox-cycling-based nanocavity device according to our previous study⁷ carried out with reference to the study of Wolfrum's group²¹ that firstly developed disk shaped nanocavity device, in an attempt to detect endotoxin rapidly and with high sensitivity. We used LGR-pAP and newly prepared Z-Leu-Gly-Arg-aminomethylferrocene (LGR-AMF) as substrates for the clotting enzyme (Fig. 1). The electrochemical signal produced by pAP and AMF, liberated from LGR-pAP and LGR-AMF, respectively, was amplified with redox cycling between the top and bottom electrodes in a nanocavity. First, we characterized the fabricated a device to estimate the signal amplification efficiency. Subsequently, we investigated the electrochemical properties of LGR-pAP and LGR-AMF using a conventional glassy carbon (GC) disc electrode. After confirming the quantitative properties of the system using a pseudo solution (mixture of LGR-pAP/pAP and LGR-AMF/AMF), we performed endotoxin assays using the fabricated device.

EXPERIMENTAL SECTION

Reagents. The Endospey ES-24S set comprised of assay buffer and LAL reagents was acquired from Seikagaku Corp. (Japan). The United States Pharmacopeia reference standard endotoxin (USP-RSE) was acquired by Seikagaku Corp. (Japan) and diluted with endotoxin-free water for injection (Otsuka Pharmaceutical Co. Ltd., Japan) to obtain the standard endotoxin solution. Immediately before use, the standard solutions were mixed by vigorous vortexing for 30 min. LGR-pAP (Watanabe Chemical Industries, Ltd., Japan) and pAP (FUJIFILM Wako Pure Chemical Corp., Japan) were dissolved in endotoxin-free water to prepare 10 mM stocks, then stored at -20 °C. LGR-AMF and AMF (Watanabe Chemical Industries, Ltd., Japan.) were dissolved in dimethyl sulfoxide (DMSO; Fujifilm Wako Pure Chemical Corp., Japan.) to obtain 10 mM stocks, then stored at -20 °C.

Fabrication of the nanocavity device. The nanocavity device was fabricated as described in Fig. S1 according to our previous study⁷. Briefly, a Ti/Pt bottom electrode, Cr sacrificial layer, and Pt top electrode were sequentially deposited onto a glass slide (Muto Pure Chemicals Co. Ltd., Japan) via sputtering (L-332S-FH, CANON ANELVA Corp., Japan) over a pattern of positive photoresist S1818G (Microchem Co., USA). After the lift-off process, an insulation layer was

1
2
3
4
5
6 fabricated on the device, except for sensor area, using negative photoresist SU-8 3050 (Microchem
7 Co., USA). Subsequently, the Cr sacrificial layer was removed by an etching solution (3% perchloric
8 acid solution containing 0.12 M ammonium hexanitratocerate (IV)). Removal of the Cr sacrificial
9 layer was confirmed by optical microscopy observation (VHX-1000, KEYENCE Corp., Japan) and
10 electrical measurement of the resistance between the top and bottom electrodes using a digital
11 voltmeter (CDM-2000D, Custom Corp., Japan). To ensure the Cr layer was completely removed, we
12 etched for an additional 25 min after the resistance was >60 k Ω . The structure of the Cr sacrificial
13 layer was characterized using atomic force microscopy (AFM; AFM5100N, Hitachi Ltd., Japan).
14
15

16 **Electrochemical measurements using the fabricated nanocavity device.**

17
18 Electrochemical measurements were performed using a multichannel potentiostat (HA-1010 mM4,
19 Hokuto Denko, Japan) with a clip connector (CCNL-050-37-FRC, Yokowo, Japan) and switching
20 matrix (NI PXI-2529, National Instruments, USA) controlled by a program written with LabVIEW
21 (National Instruments). A sample solution was introduced onto the sensor area and Ag/AgCl (sat.
22 KCl) as a reference electrode and counter electrode were inserted into the solution. After the
23 experiment, the device was washed using Milli-Q water (Millipore Corp., Billerica, MA, USA) for
24 repeated use.
25
26
27
28
29

30 **Electrochemical measurement using a GC electrode.** The electrochemical properties of
31 LGR-pAP, pAP, LGR-AMF and AMF were characterized using a GC disk electrode 1.0 mm in
32 diameter (BAS Inc., Tokyo, Japan), Ag/AgCl (sat. KCl) reference electrode, and counter electrode
33 (Pt wire 0.3 mm in diameter, 99.99%, Tanaka Kikinzoku Kogyo Co. Ltd., Japan). The sample
34 solutions were prepared in 10 mM HEPES buffer containing 0.1 M KCl (pH 7.8).
35
36

37 **Electrochemical endotoxin assay using the fabricated devices.** The LAL solutions were
38 prepared by adding 180 μ L the Endospey assay buffer and 20 μ L of 10 mM LGR-pAP or
39 LGR-AMF stock solution to a test vial from the Endospey set containing lyophilized LAL reagents.
40 After mixing 200 μ L of LAL solution with 200 μ L of the endotoxin solution, this LAL assay
41 solution was incubated at 37 $^{\circ}$ C for 1 h or 30 min. After incubation, 200 μ L of the LAL assay
42 solution was applied onto the device and measured immediately. After the experiment, the devices
43 were dipped into an alkaline detergent (2% white 7-RT solution; Yuai Kasei Co. Ltd., Japan) for 30
44 min to remove the adsorbed protein from the electrode surface and subsequently rinsed with Milli-Q
45 water. All procedures for endotoxin detection were performed in a laminar flow cabinet to prevent
46 endotoxin contamination.
47
48
49
50
51
52
53

54 **RESULTS AND DISCUSSION**

55 **Device fabrication.** Fig. 2A and 2B show optical microscope images of the fabricated
56 device and a cross-sectional illustration, respectively. The fabricated device consisted of top-ring and
57 bottom-ring electrodes with a nanocavity between them. When the nanocavity was filled with a
58
59
60

1
2
3
4
5
6 sample solution containing redox species, redox cycling occurred between the top and bottom
7 electrodes biased at appropriate oxidation and reduction potentials, respectively. To estimate the
8 cavity height, we obtained an AFM image (Fig. 2C) before covering the device with an SU-8
9 insulation layer (Fig. S1 iii). Fig. 2D shows a one-line scan profile of the AFM image from the
10 inside of the ring to the outside at the lead portion, as indicated by the red dotted line in Fig. 2C.
11 Fig. 2E shows a schematic illustration of a cross-sectional structure corresponding to Fig. 2D. Dips
12 at the corner of the steps of the lead part in Fig. 2D is assumed to be caused by the shadowing effect
13 on spattering. From the AFM image, the sacrificial layer thickness was determined to be 190 nm,
14 which is the height of nanocavity between the two electrodes after removal of the sacrificial layer.
15
16
17
18

19 **Characterization of the device.** The fabricated device was characterized with cyclic
20 voltammetry using 500 μM ferrocenemethanol (FMA; Sigma-Aldrich Co. LLC.) dissolved in a 0.1
21 M KCl solution. First, cyclic voltammetry was performed with redox cycling. The potential of the
22 top electrode was swept at a scan rate of 20 mV/s, while the applied potential of the bottom electrode
23 was biased at 0.0 V. Under these conditions, sigmoidal voltammograms with steady-state currents
24 (± 530 nA) were obtained from the top and bottom electrodes (Fig. 3a and 3b). Next, the cyclic
25 voltammetry with non-redox-cycling condition was simulated using COMSOL Multiphysics
26 (version 5.4, COMSOL, Inc., USA) using a model of the nanocavity device without the bottom
27 electrode. The reason why we examined by simulation instead of experiment is to avoid having to
28 fabricate a second set of devices without a bottom electrode, because the presence of the bottom
29 electrode, even if unconnected, would induce the redox cycling (called self-redox cycling²⁰) between
30 the potential-applied top electrode and floating bottom electrode. To avoid the influence of the
31 self-redox cycling on the evaluation of redox efficiency without having to fabricate a second set of
32 devices, we employed the simulation. The diffusion coefficients of FMA and FMA⁺ were set as 7.0
33 $\times 10^{-6}$ cm²/s and the formal redox potential of the FMA was set as 0.216 V with a scan rate of 20
34 mV/s. The voltammogram of the non-redox-cycling condition from the simulation is shown in Fig.
35 3c. From this sigmoidal voltammogram, the steady-state current with 320 pA was obtained. These
36 result show that the electrochemical current is amplified with redox-cycling by 1660 times using the
37 fabricated device compared to non-redox cycling condition. The cycling efficiency (cathodic current
38 / anodic current) under the redox-cycling conditions is 98%. This suggests that almost all of the
39 oxidant generated at the top electrode reach the bottom electrode to be reduced. These results clearly
40 show that our nanocavity device can be used for a highly sensitive sensor.
41
42
43
44
45
46
47
48
49
50
51

52 **Electrochemical characterization of the substrates.** The electrochemical properties of
53 the substrates used in this study were characterized. First, we performed cyclic voltammetry using
54 500 μM LGR-pAP and 500 μM pAP (Fig. 4A) in addition to 500 μM LGR-AMF and 500 μM AMF
55 (Fig. 4B) using a GC electrode at a scan rate of 20 mV/s for basic characterization of the substrates
56 and liberated molecules after the LAL reaction. As shown in Fig. 4A, LGR-pAP showed an
57
58
59
60

1
2
3
4
5
6 irreversible voltammogram with an oxidation peak at 0.64 V (Fig. 4Aa). In contrast, pAP showed a
7 reversible voltammogram with a formal potential at 0.08 V and oxidation peak potential at 0.16 V
8 (Fig. 4Ab). These results indicate that the redox-cycling can amplify the signal of liberated pAP
9 without amplification of LGR-pAP by using 0.5 V and -0.2 V as potentials applied to the top and
10 bottom electrodes of the nanocavity device, respectively. On the other hand, both LGR-AMF and
11 AMF showed reversible-shaped voltammograms with formal potentials at 0.28 and 0.38 V,
12 respectively (Fig. 4Ba and b, respectively). The difference in the formal potential of 0.1 V is not
13 sufficient to distinguish AMF from LGR-AMF by redox cycling. Therefore, we examined a method
14 using the difference in diffusion coefficients between LGR-AMF and AMF, assuming that this
15 difference should be reflected in the amplification efficiency during redox-cycling, resulting in an
16 AMF concentration-dependent current output from the nanocavity device. The diffusion coefficients
17 of LGR-AMF and AMF were estimated using the Randles-Sevcik equation (Eq. (1)) with peak
18 currents obtained from the cyclic voltammograms at different scan rates (Fig. 4C and D).

$$i_p = 0.4463nFAC\sqrt{\frac{nFvD}{RT}} \quad (1)$$

19
20
21
22
23
24
25
26
27
28 In Eq. (1), i_p represents the peak current (A), n is the number of charges involved in the
29 electrochemical half-reaction, F is Faraday's constant (96,485 C/mol), A is the electrode area
30 (cm^2), C is the molar concentration of AMF or LGR-AMF in the electrolyte (mol/cm^3), v is the scan
31 rate (V/s), D is the diffusion coefficient of AMF or LGR-AMF (cm^2/s), R is the universal gas
32 constant (8.314 J/mol·K), and T is the absolute temperature (K). Upon plotting the peak currents
33 obtained at different scan rates against the square root of the sweep rate, the diffusion coefficient
34 were obtained as a slope of the linear graph (Fig. 4Da and b). The calculated diffusion coefficients of
35 LGR-AMF and AMF were 2.89×10^{-6} and 6.92×10^{-6} cm^2/s , respectively. AMF exhibited a diffusion
36 coefficient 2.39 times larger than that of LGR-AMF, indicating the potential for detecting AMF
37 liberated from LGR-AMF by differences in redox cycling efficiency in the nanocavity device.

38
39
40
41
42
43 Voltammetric studies in the fabricated nanocavity device were then performed using 500
44 μM LGR-pAP, pAP, LGR-AMF, and AMF to determine the electrochemical dynamics of the
45 molecules in the nanocavity. The potential of the top electrode was swept while the bottom electrode
46 was biased at a constant potential. The cyclic voltammograms of LGR-pAP and pAP from the top
47 and bottom electrodes with the bottom electrode biased at -0.2 V are shown in Fig. 5A. Compared to
48 the cyclic voltammograms of FMA (Fig. 3), those of LGR-pAP and pAP were less ideal sigmoid
49 curves. This indicates that poorly conductive substances derived from LGR-pAP and pAP adsorbed
50 to the electrode surfaces inhibited electron transfer. The redox current of LGR-pAP only slightly
51 increased from -0.2 to 0.8 V, whereas the redox current of pAP significantly increased from 0.22 V
52 to exceed the current of LGR-pAP. From Fig. 5A, we employed 0.5 V vs Ag/AgCl as the potential
53 applied to the top electrode for amperometric detection of pAP liberated from LGR-pAP. On the
54
55
56
57
58
59
60

1
2
3
4
5
6 other hand, both the cyclic voltammograms of LGR-AMF and AMF showed sigmoid curves with
7 clear steady-state currents at >0.5 V (Fig. 5B) when the bottom electrode was biased at 0.0 V. The
8 formal potentials of both LGR-AMF and AMF were shifted to 0.1 V positive side from those
9 obtained with GC disk electrode (Fig. 4B). We consider this formal potential shift is due to the
10 requirement of extra voltages for redox reaction at the electrode surfaces in the nanocavity,
11 especially at parts far from the device opening, because the formation of the electric double layer
12 was inhibited due to the restriction of the ion movement. From the result shown in Fig. 5B, 0.5 V vs
13 Ag/AgCl was used as the potential applied to the top electrode for amperometric detection of AMF
14 liberated from LGR-AMF.
15
16
17
18

19 **Demonstration of nanocavity device using endotoxin model solution.** Before the
20 endotoxin assay, we demonstrated the quantitative detection of liberated pAP and AMF from
21 LGR-pAP and LGR-AMF using the nanocavity device with model solutions. The model solutions,
22 prepared by mixing 500 μ M pAP (or AMF) and 500 μ M LGR-pAP (or LGR-AMF) with changing
23 mixing ratios simulated the state of the solution after the LAL reaction. 10 mM HEPES (pH 7.8) and
24 0.1 M KCl were added to the model solutions.
25
26
27

28 Fig. 6A shows the amperograms of the mixed solutions of pAP and LGR-pAP obtained
29 from the bottom electrode of the nanocavity device. The current of the bottom electrode biased at
30 -0.2 V was monitored, while the potential applied to the top electrode was stepped from -0.2 to 0.5 V
31 at 10 s. After the potential step of the top electrode, the monitored current increased and gradually
32 equilibrated to a constant current. The constant currents increased with increasing pAP content in the
33 mixed solutions. These results indicate that redox cycling successfully occurred between the bottom
34 electrode at -0.2 V and the top electrode at 0.5 V to amplify the signal from pAP. Fig. 6B shows the
35 calibration plots obtained using the average current 50–60 s after subtracting the average of the
36 current at 9–9.96 s. The obtained liner calibration plot showed that our nanocavity device can
37 quantify pAP in the presence of LGR-pAP.
38
39
40
41
42

43 Fig. 6C shows the amperograms of the mixed solutions of AMF and LGR-AMF obtained
44 in the same manner as those of the pAP and LGR-pAP mixtures, but the bottom electrode was biased
45 at 0.0 V and the potential applied to the top electrode was stepped from 0.0 to 0.5 V at 10 s. After the
46 potential step of the top electrode, the spiked current was monitored and gradually decreased until
47 reaching to a constant current. The constant currents increased with increasing AMF content in the
48 mixed solutions. Fig. 6D shows the calibration plots used for the current that subtract the average
49 current at 9–9.96 s from the average current at 50–60 s. The 100 nA of the y-intercept of the linear
50 calibration plot represents the amplified signal of the 500 μ M LGR-AMF. This result indicates that
51 the concentration of AMF liberated from LGR-AMF of known concentration can be accurately
52 estimated using the nanocavity device due to the difference in diffusion coefficients between AMF
53 and LGR-AMF. This is a novel analytical method that has not been reported to date. We show for
54
55
56
57
58
59
60

1
2
3
4
5
6 the first time that analytes can be detected by differences in diffusion coefficients using a device
7 with high redox cycling efficiency, such as a nanocavity device.

8
9 Unlike ideal redox cycling in a nano-space, Fig. 6A and 6C indicate that steady-state is not
10 achieved quickly. Under ideal conditions, the time to reach the steady-state should be instantaneous
11 for the nanocavity device because a constant diffusion layer between two electrodes should be
12 formed within a short period. The long time required to reach the steady-state is likely caused by
13 adsorption and desorption of the redox species on the electrode surfaces.²¹ The difference in the
14 aerogram shape between 500 μM pAP and 500 μM AMF (for pAP, the current gradually increased
15 and reached steady-state, whereas in for AMF, the current gradually decreased after the large pulsed
16 current and reached a steady-state) can be explained by adsorption and desorption of the redox
17 species on the electrode surfaces.²² For pAP, after the potential of the top electrode was stepped,
18 some redox molecules likely adsorbed on the electrode surfaces, temporally decreasing the redox
19 molecule concentration between the two electrodes. Gradually, redox molecules would be supplied
20 from the outside bulk solution, allowing the steady-state to be reached. On the other hand, for AMF,
21 before the potential of the top electrode was stepped, some redox molecules likely adsorbed on the
22 electrode surfaces. After the potential step, the adsorbed molecules likely desorbed from the
23 electrodes, temporally increasing the redox molecule concentration between two electrodes until
24 reaching the steady-state.

25
26
27
28
29
30
31
32 **Endotoxin assay using the fabricated device.** Finally, the endotoxin assay was
33 performed using the fabricated device. First, we performed the endotoxin assay using LGR-pAP as a
34 substrate for LAL. A 200 μL LAL solution containing 1 mM LGR-pAP and 200 μL of the endotoxin
35 solution were mixed in a test tube and incubated at 37 $^{\circ}\text{C}$ for 1 h. After incubation, 200 μL of the
36 solution was introduced to the nanocavity device. The current from the bottom electrode biased at
37 -0.2 V was monitored while the potential applied to the top electrode was stepped from -0.2 to 0.5 V
38 at 10 s. The amperograms obtained from the bottom electrode are shown in Fig. 7A. The calibration
39 plot obtained using the current value that subtracted the average current of 9 to 9.96 s from that of 50
40 to 60 s is shown in Fig. 7B. The error bars indicate the standard deviations obtained from triplicate
41 measurements. Fig. 7C is a magnified graph of Fig. 7B at 0–10 EU/L. From these results, the current
42 signal clearly increased with increasing endotoxin concentration. The limit of detection (LOD) was
43 calculated as the concentration that corresponded to 3 times the standard deviation of the 0 EU/L and
44 was 0.2 EU/L after 1 h of the LAL reaction using LGR-pAP. The endotoxin detection range under
45 these condition was determined to be 0.2–10,000 EU/L. In order to examine endotoxin assay in
46 shorter time, the same experiment was performed with a LAL reaction time of 30 min. The obtained
47 amperograms and calibration plots are shown in Fig. 7D and E, respectively. Fig. 7F is a magnified
48 graph of Fig. 7E at 0–100 EU/L. The LOD in case of 30 min of the LAL reaction using LGR-pAP
49 was 0.5 EU/L and the detection range was 0.5–10,000 EU/L. Comparing to our previous study using
50
51
52
53
54
55
56
57
58
59
60

1
2
3
4
5
6 LGR-pAP substrate without redox cycling¹⁶, the sensitivities were increased 5 and 200-fold for 30
7 min and 1 h of LAL reaction time, respectively. These results indicate that the fabricated nanocavity
8 device can be used as a highly sensitive endotoxin sensor with LGR-pAP as a substrate for the LAL
9 reaction.
10

11 Next, the endotoxin assay using LGR-AMF substrate was performed in the same manner,
12 but the step potential for the top electrode was 0 to 0.5 V and the bottom electrode was biased at 0 V.
13 However, no significant difference in current signal was observed with changing endotoxin
14 concentration from 0 to 100 EU/L (Fig. S2). 100000 and 0 EU/L of endotoxin solutions also showed
15 no significant difference in current signal. We assume that the clotting enzyme did not react with
16 LGR-AMF probably because of the steric hindrance of the bulky AMF. This is not a critical problem
17 and can be solved by further design of the substrate. We are now modifying the LGR-AMF substrate
18 to more easily react with the clotting enzyme. We believe that the result can be reported in near
19 future.
20
21
22
23
24
25

26 CONCLUSION

27 In this study, we developed a novel electrochemical method for the highly sensitive and
28 rapid detection of endotoxin based on the LAL reaction with signal amplification by redox cycling
29 between a pair of electrodes in a nanocavity. From the AFM images, the fabricated nanocavity
30 device contained a 190-nm gap between the top and bottom electrodes. The electrochemical
31 properties of the fabricated nanocavity device were characterized using 500 μM FMA, showing a
32 cycling efficiency of 98% and an amplification rate of 1660-fold with redox cycling. We also
33 characterized the electrochemical properties of the LGR-pAP, pAP, LGR-AMF and AMF using a
34 GC disc electrode. The results indicated that pAP liberated from LGR-pAP can be detected using
35 their redox potential difference, while AMF liberated from LGR-AMF can be detected using their
36 diffusion coefficient difference even though LGR-AMF and AMF have nearly identical formal
37 potentials. Before the endotoxin assay, we demonstrated the quantitative detection of pAP and AMF
38 using the fabricated nanocavity device in the presence of LGR-pAP and LGR-AMF, respectively,
39 using mixed solutions of LGR-pAP and pAP (and mixed solutions of LGR-AMF and AMF) as
40 model for the LAL reaction solutions. We obtained linear calibration plots for the concentration of
41 the pAP in the presence of LGR-pAP by amplifying the signal of pAP via redox cycling. We also
42 successfully obtained a linear calibration plot with respect to the concentration of the AMF in the
43 presence of LGR-AMF utilizing the difference in their diffusion coefficients. We finally performed
44 the endotoxin assay using the fabricated nanocavity device. The electrochemical signal from pAP
45 increased with increasing endotoxin concentration when LGR-pAP was used as a substrate for the
46 LAL reaction. The LOD was 0.2 and 0.5 EU/L for the LAL reaction times of 1 h and 30 min,
47 respectively. However, endotoxin assay using the LGR-AMF substrate was not successful likely
48
49
50
51
52
53
54
55
56
57
58
59
60

1
2
3
4
5
6 because the clotting enzyme did not react with LGR-AMF. Now we are modifying the LGR-AMF
7 substrate to more readily react with the clotting enzyme. For the future application, actual sample
8 test is important. We would proceed the application study of our device and strategy to real samples
9 that require highly sensitive endotoxin management such as dialysate, pharmaceuticals and human
10 plasma. We conclude that endotoxin detection with highly efficient redox-cycling using a nanocavity
11 device can provide a highly sensitive and simple platform to ensure safety for dialysis therapy.
12
13
14
15

16 **Acknowledgments**

17 This research is partially supported by the Center of Innovation Program of the Japan Science and
18 Technology Agency, JST. It is also partly supported by a Grant-in-Aid for Scientific Research (A)
19 (No. 89000161) from JSPS.
20
21
22

23 **REFERENCES**

- 24 (1) F. R. F. Fan, A. J. Bard, *Science*, **1995**, *267*, 871-874
- 25 (2) F. R. F. Fan, J. Kwak, A. J. Bard, *J. Am. Chem. Soc.*, **1996**, *118*, 9669-9675
- 26 (3) P. Sun, M. V. Mirkin, *J. Am. Chem. Soc.*, **2008**, *130*, 8241-8250
- 27 (4) M. A. G. Zevenbergen, P. S. Singh, E. D. Goluch, B. L. Wolfrum, S. G. Lemay, *Nano Lett*, **2011**,
28 *11*, 2881-2886
- 29 (5) S. Kang, A. F. Nieuwenhuis, K. Mathwig, D. Mampallil, S. G. Lemay, *ACS Nano*, **2013**, *12*,
30 10931-10937
- 31 (6) J. C. Byers, B. P. Nadappuram, D. Perry, K. McKelvey, A. W. Colburn, P. R. Unwin, *Anal.*
32 *Chem.*, **2015**, *87*, 10450-10456
- 33 (7) Y. Kanno, K. Ino, H. Shiku, T. Matsue, *Lab Chip.*, **2015**, *15*, 4404-4414
- 34 (8) E. T. Rietschel, T. Kirikae, F. U. Schade, U. Mamat, G. Schmidt, H. Loppnow, A. J. Ulmer, U.
35 Z'ahringer, U. Seydel, F. D. Padova, M. Schreier H. Brade, *FASEB J.*, **1994**, *8*, 217-225.
- 36 (9) R. B. Yang, M. R. Mark, A. Gray, A. Huang, M. H. Xie, M. Zhang, A. Goddard, W. I. Wood, A.
37 L. Gurney P. J. Godowski, *Nature*, **1998**, *395*, 284-288.
- 38 (10) M. Mineshima, H. Kawanishi, T. Ase, T. Kawasaki, T. Tomo, *Renal Replac. Ther.*, **2018**, *4*:15
- 39 (11) S. Nakamura, T. Morita, S. Iwanaga, M. Niwa, K. Takahashi, *J. Biochem.*, **1977**, *81*, 1567-1569
- 40 (12) J. Scudder, J. Y. Ye, *J. Biomed. Opt.*, **2018**, *23*, 27001-27007
- 41 (13) D. Takahashi, S. Hachuda, T. Watanabe, Y. Nishijima, T. Baba, *Appl. Phys. Lett.*, **2015**, *106*,
42 13112-13115
- 43 (14) K. Y. Inoue, K. Ino, H. Shiku, T. Matsue, *Electrochem, Commun.*, **2010**, *12*, 1066-1069
- 44 (15) K. Y. Inoue, S. Takahashi, K. Ino, H. Shiku, T. Matsue, *Innate Immun.*, **2011**, *18*, 343-349
- 45 (16) K. Y. Inoue, S. Takano, S. Takahashi, Y. Ishida, K. Ino, H. Shiku, T. Matsue, *Analyst*, **2013**,
46 *138*, 6523-6531
- 47
48
49
50
51
52
53
54
55
56
57
58
59
60

- 1
2
3
4
5
6 (17) S. Takanno, K. Y. Inoue, S. Takahashi, K. Ino, H. Shiku, T. Matsue, *Analyst*, **2014**, *139*,
7 5001-5006
8
9 (18) S. Takano, K. Y. Inoue, M. Ikegawa, Y. Takahashi, K. Ino, H. Shiku, T. Matsue, *Electrochem.*
10 *Commun.*, **2016**, *66*, 34-37
11
12 (19) A. Oda, D. Kato, K. Yoshioka, M. Tanaka, T. Kamata, M. Todokoro, O. Niwa, *Electrochim.*
13 *Acta*, **2016**, *197*, 152-158
14
15 (20) T. Horiuchi, O. Niwa, M. Morita, H. Tabei, *J. Electrochem. Soc.*, **1991**, *138*, 3549-3553
16
17 (21) E. Kätelhön, B. Hofmann, S. G. Lemay, M. A. G. Zevenbergen, A. Offenhäusser, B. Wolftrum,
18 *Anal. Chem.*, **2010**, *82*, 8502-8509
19
20 (22) S. Kang, K. Mathwig, S. G. Lemay, *Lab Chip*, **2012**, *12*, 1262-1267
21
22
23
24
25
26
27
28
29
30
31
32
33
34
35
36
37
38
39
40
41
42
43
44
45
46
47
48
49
50
51
52
53
54
55
56
57
58
59
60

FIGURE CAPTIONS

Figure 1. Principles of the LAL-based electrochemical assay with redox-cycling in a nanocavity.

Figure 2. Optical microscope image of the top view of the nanocavity device (A) and cross-sectional illustrations of the nanocavity device (B). An AFM image of the device before covering with the insulation layer (C) and one line scan AFM result (D) with an illustration of the cross-sectional view of corresponding part (E).

Figure 3. Cyclic voltammograms of 500 μM FMA in 0.1 M KCl for characterization of the fabricated nanocavity device. Voltammograms under redox-cycling conditions were obtained from the top (a) and bottom electrodes (b) by scanning the potential of the top from 0 to 0.6 V at 20 mV/s, while the bottom electrode was biased at 0.0 V. Simulated voltammograms under non-redox-cycling conditions (c) was obtained using the COMSOL Multiphysics program with a model of the nanocavity device without the bottom electrode. The inset shows a magnified graph of (c).

Figure 4. Substrate characterization by cyclic voltammetry with a GC electrode. (A) Cyclic voltammograms of (a) 500 μM LGR-pAP and (b) 500 μM pAP, at a scan rate of 20 mV/s. (B) Cyclic voltammograms of (a) 500 μM LGR-AMF and (b) 500 μM AMF, at a scan rate of 20 mV/s. (C) Cyclic voltammograms of (a) LGR-AMF and (b) AMF at scan rates of (i) 4, (ii) 20, (iii) 50, and (iv) 100 mV/s. (D) Randles-Sevcik plots used for the estimation of the diffusion coefficients of LGR-AMF (a) and AMF (b).

Figure 5. (A) Cyclic voltammograms of pAP (a and b) and LGR-pAP (c and d) obtained from the top (a and c) and bottom electrodes (b and d) of the fabricated device by scanning the potential of the top electrode while the bottom electrode was biased at -0.2 V vs. Ag/AgCl. (B) Cyclic voltammograms of AMF (a and b) and LGR-AMF (c and d) obtained from the top (a and c) and bottom electrodes (b and d) of the fabricated device by scanning the potential of the top electrode while the bottom electrode was biased at 0.0 V vs. Ag/AgCl.

Figure 6. (A) Amperograms obtained from the bottom electrode of the fabricated device for the model solutions. The model solutions were prepared by mixing 500 μM of LGR-pAP and 500 μM of pAP in 10 mM HEPES containing 0.1 M KCl with respective mixing ratios of (a) 1:0, (b) 0.75:0.25, (c) 0.5:0.5, (d) 0.25:0.75, and (e) 0:1. The potential of the top electrode was stepped from -0.2 to 0.5 V while the bottom electrode was maintained at -0.2 V. (B) Calibration plot for pAP in the model solution. The plotted value was calculated by subtracting the average current of 9–9.96 s from the average current of 50–60 s. Error bars represent standard deviations ($n=3$). (C) Amperograms

1
2
3
4
5
6 obtained from the bottom electrode of the device for the endotoxin model solution containing
7 LGR-AMF and AMF. The mixture ratios of 500 μ M LGR-AMF and AMF were (a) 1:0, (b)
8 0.75:0.25, (c) 0.5:0.5, (d) 0.25:0.75, and (e) 0:1, respectively. The top electrode was stepped from 0
9 to 0.5 V while the bottom electrode was biased at 0 V. (D) Calibration plot for AMF in the model
10 solution. The plots and error bars were made in the same manner as described in (B).
11
12
13

14
15 Figure 7. (A) Amperograms obtained from the bottom electrode of fabricated device for the
16 endotoxin assay using LGR-pAP after 1 h of LAL reaction time. The top electrode was stepped from
17 -0.2 to 0.5 V versus Ag/AgCl at 10 s while the bottom electrode was biased at 0 V. The endotoxin
18 concentrations of the samples were (a) 0, (b) 1, (c) 10, (d) 100 and (e) 1000 EU/L. (B) Calibration
19 plot for endotoxin using LGR-pAP with 1 h of LAL reaction time. The plotted value was calculated
20 by subtracting the average current of 9–9.96 s from the average current of 50–60 s. Error bars
21 represent standard deviations (n=3) (C) Magnified graph of (B) at 0–10 EU/L. (D) The amperograms
22 obtained in same manner as (A) but the LAL reaction time of 30 min. The endotoxin concentrations
23 of the samples were (a) 0, (b) 1, (c) 10, (d) 100, and (e) 1000 EU/L. (E) Calibration plot for
24 endotoxin using LGR-pAP after 30 min of LAL reaction time. The plots and error bars were made in
25 the same manner as described in (B). (F) Magnified calibration plot of (D).
26
27
28
29
30
31
32
33
34
35
36
37
38
39
40
41
42
43
44
45
46
47
48
49
50
51
52
53
54
55
56
57
58
59
60

Fig.1

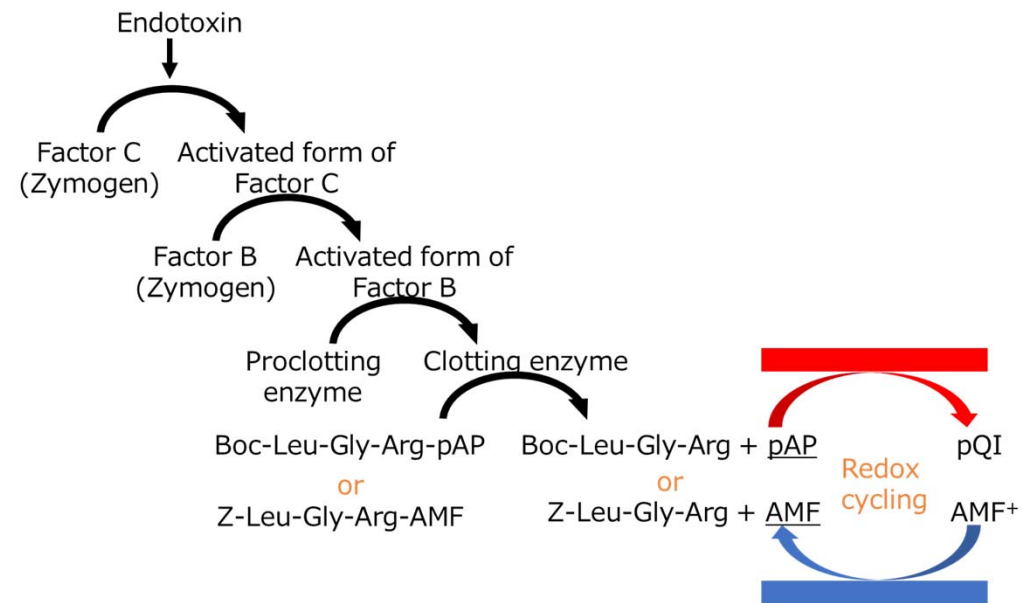


Fig.2

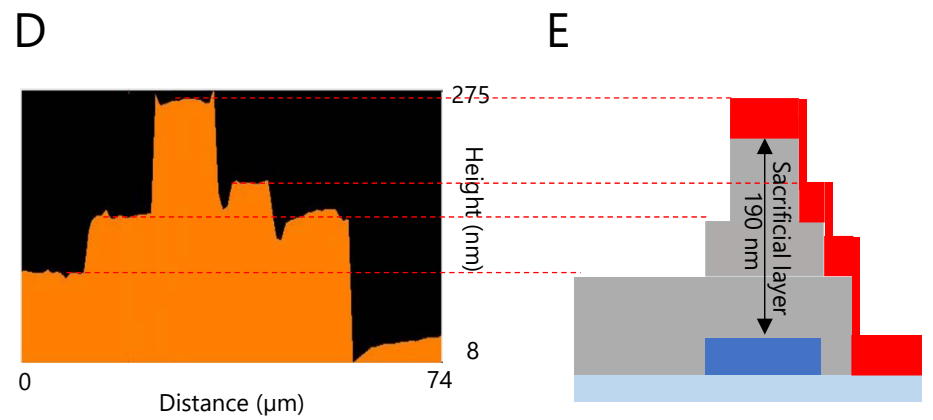
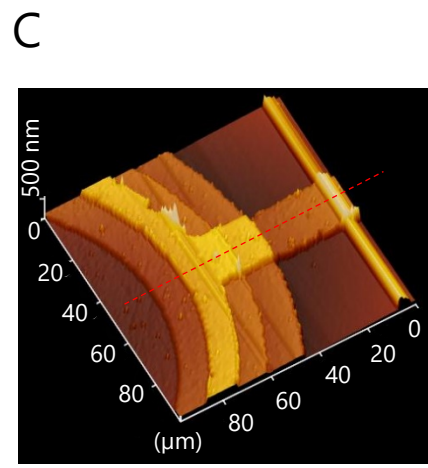
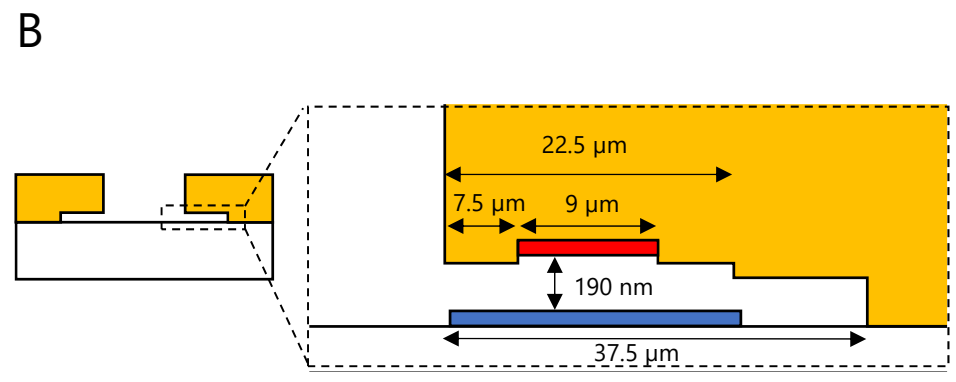
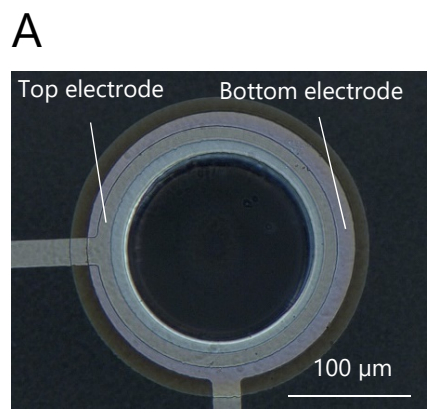


Fig.3

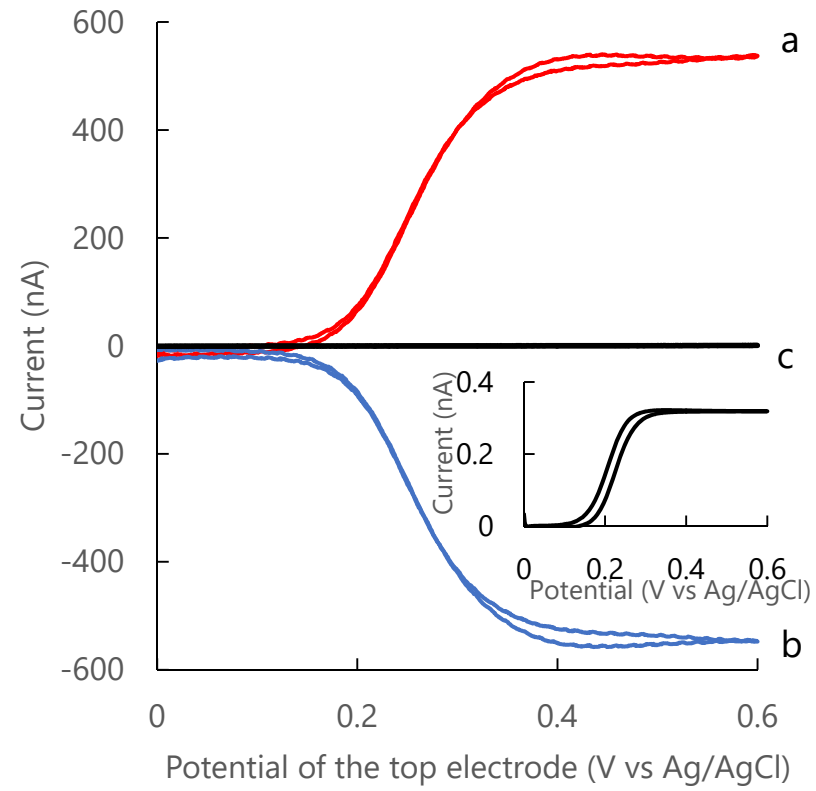


Fig.4

1
2
3
4
5
6
7
8
9
10
11
12
13
14
15
16
17
18
19
20
21
22
23
24
25
26
27
28
29
30
31
32
33
34
35
36
37
38
39
40
41
42
43
44
45
46

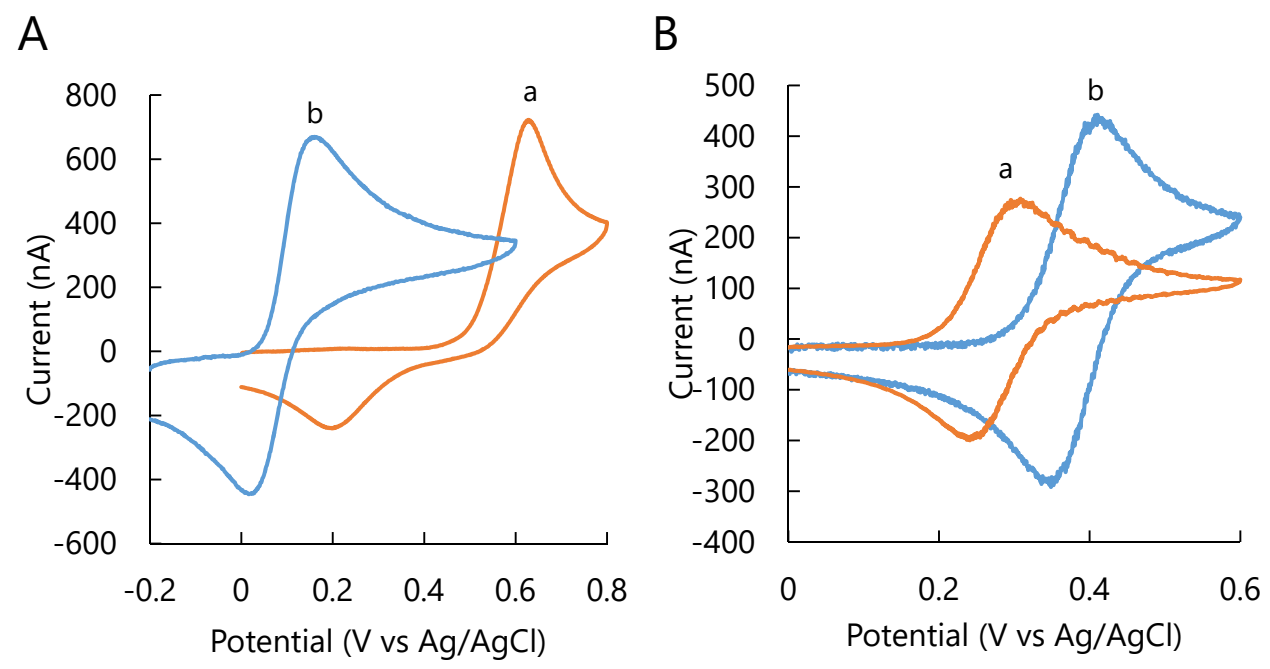


Fig.4 (Continued)

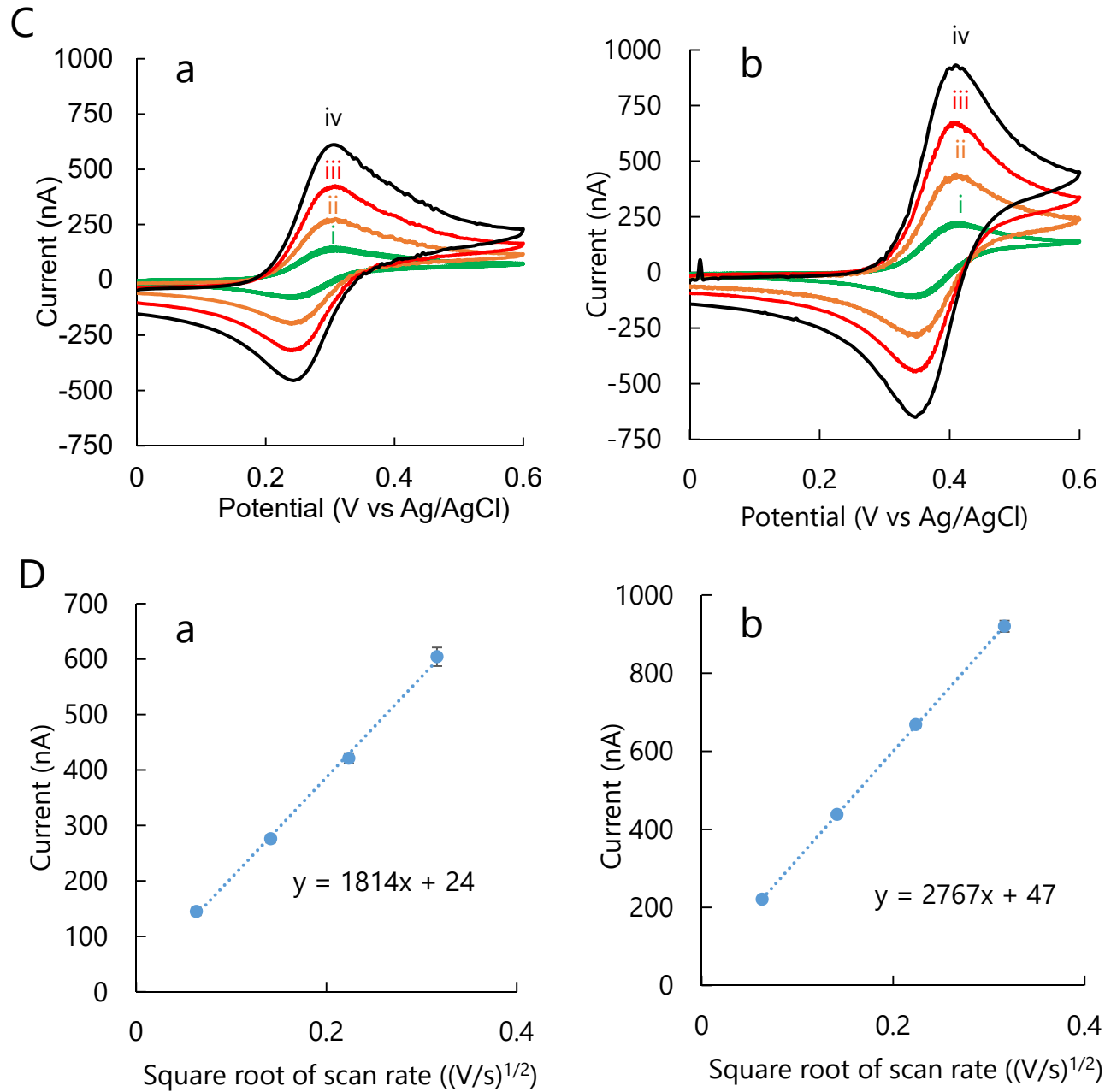


Fig.5

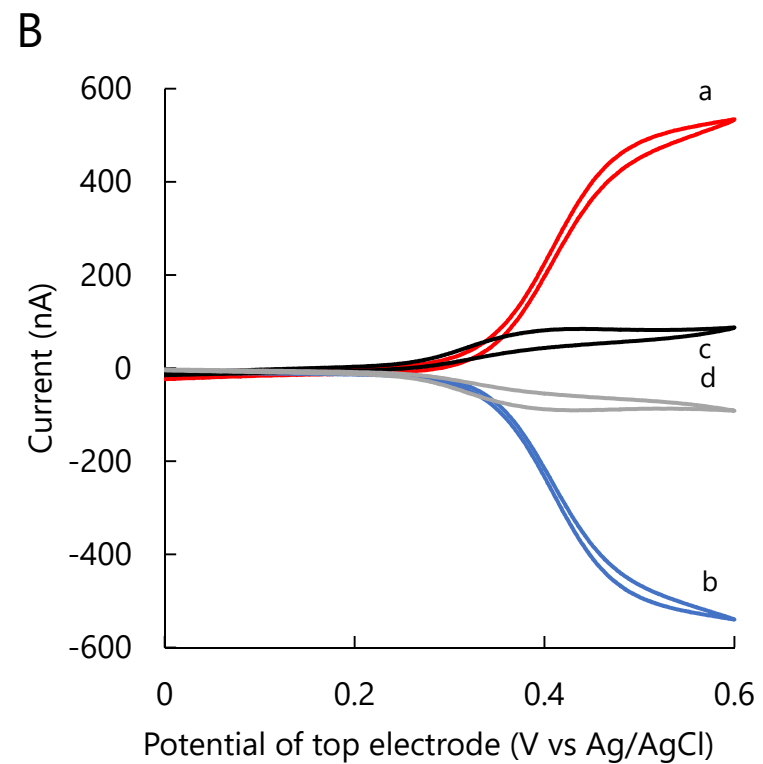
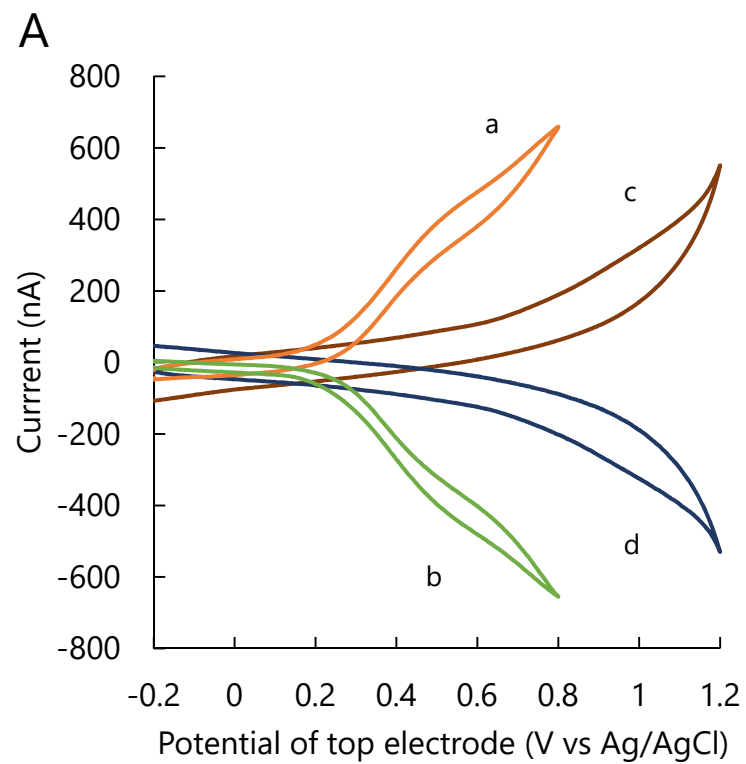


Fig.6

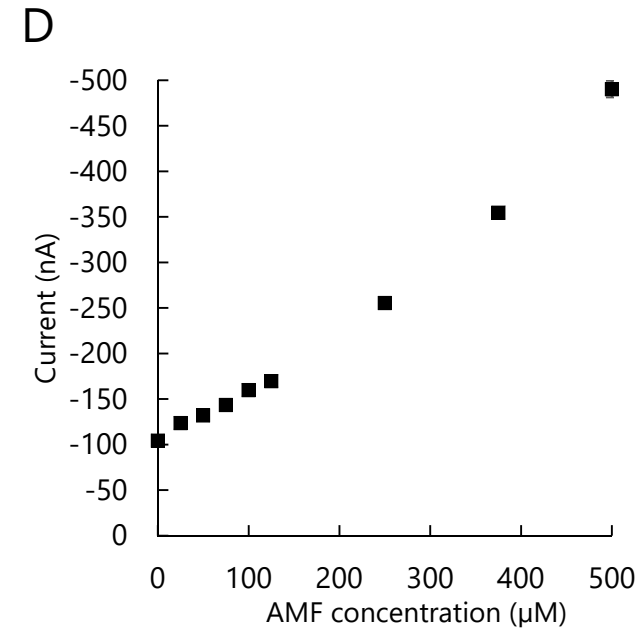
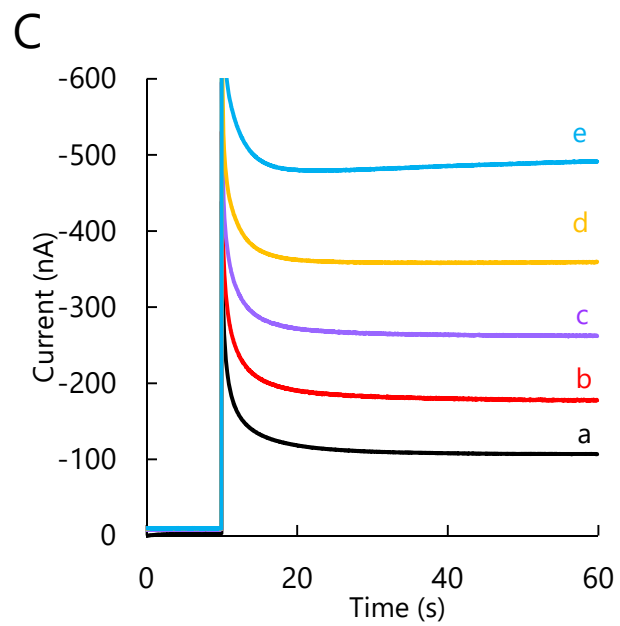
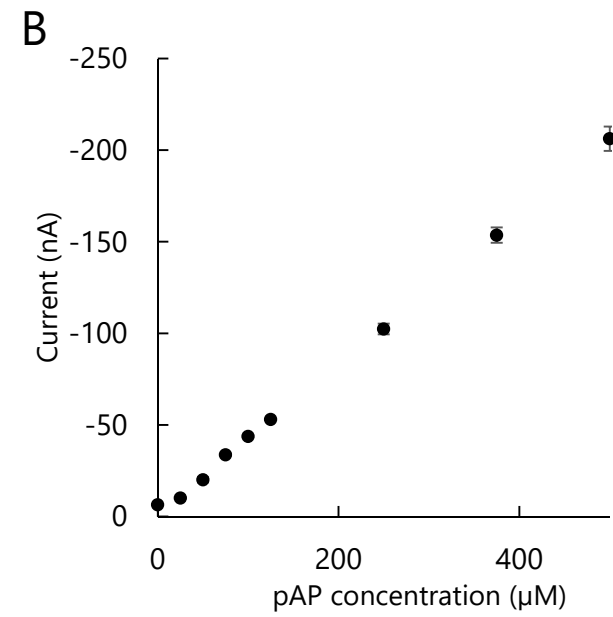
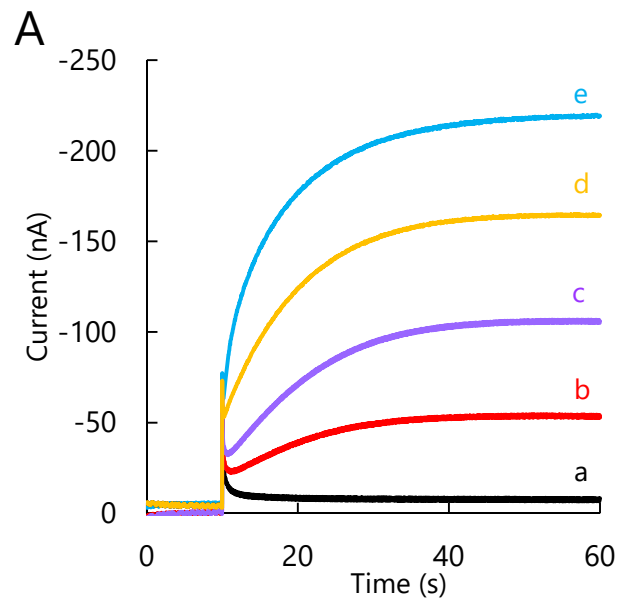


Fig.7

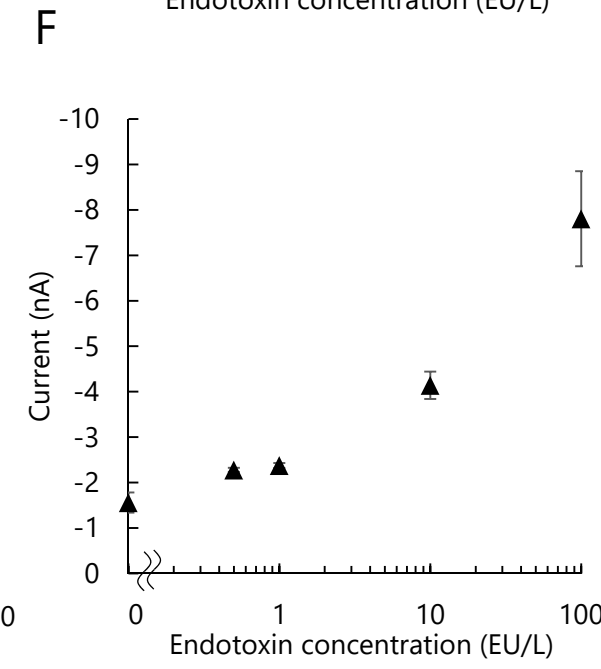
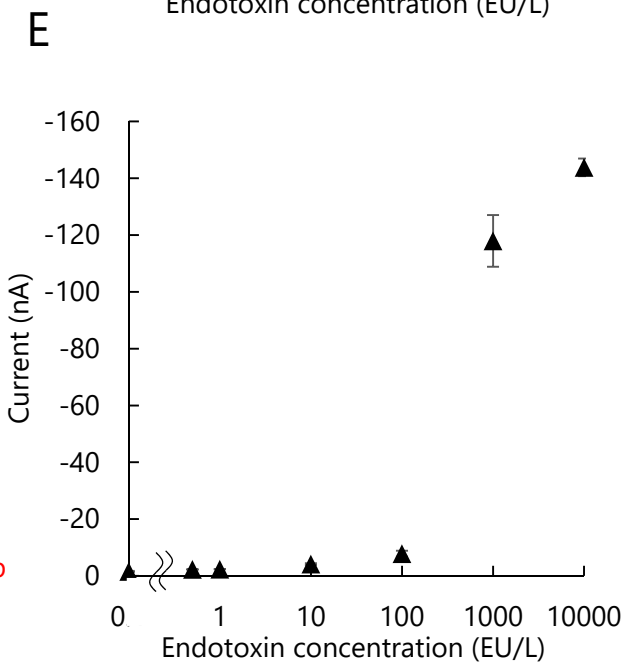
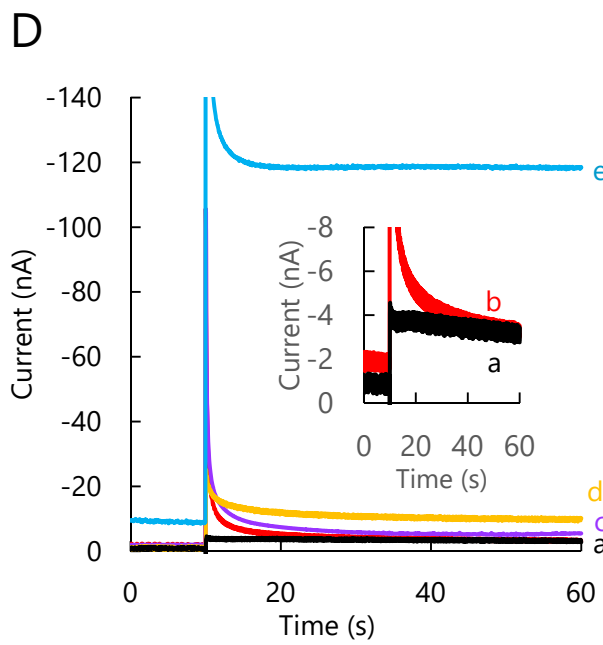
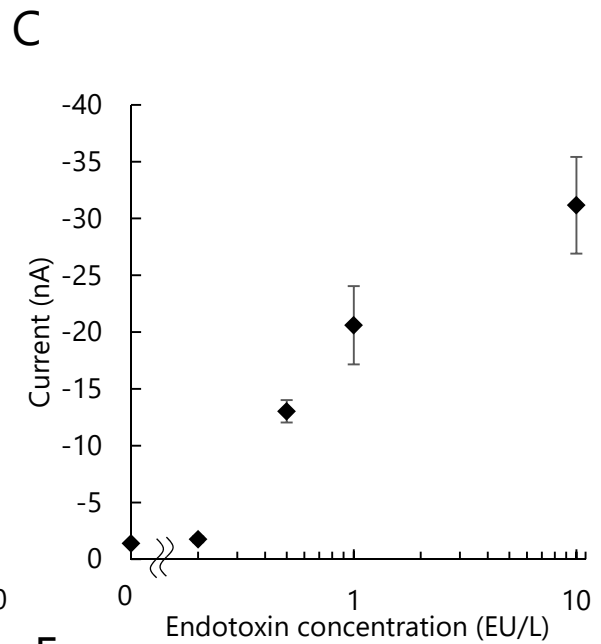
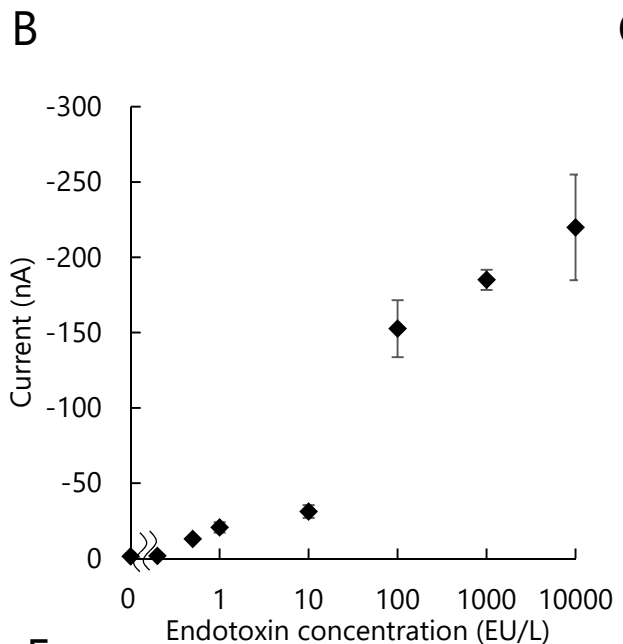
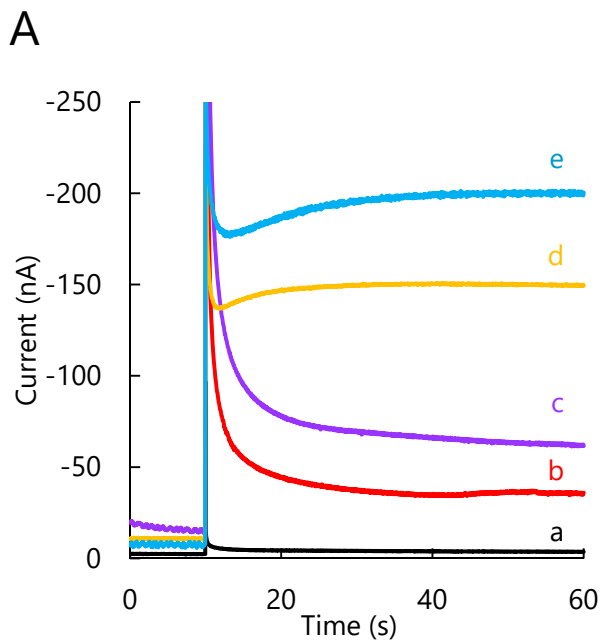
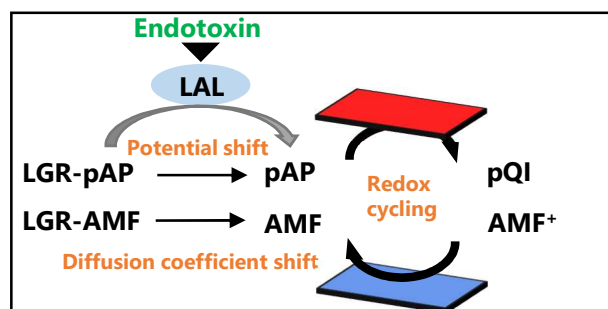


Table of contents



A highly sensitive endotoxin sensor and a novel analytical principle using diffusion coefficient difference was developed with a nanocavity device